Zn-doped SnO2 nanocrystals as efficient DSSC photoanode material and remarkable photocurrent enhancement by interface modification

Dou, Xincun; Prabhakar, Rajiv Ramanujam; Mathews, Nripan; Lam, Yeng Ming; Mhaisalkar, Subodh Gautam

2012

Dou, X., Prabhakar, R. R., Mathews, N., Lam, Y. M., & Mhaisalkar, S. (2012). Zn-Doped SnO2 Nanocrystals as Efficient DSSC Photoanode Material and Remarkable Photocurrent Enhancement by Interface Modification. Journal of The Electrochemical Society, 159(9), H735-H739.

https://hdl.handle.net/10356/97697

https://doi.org/10.1149/2.032209jes

Journal of The Electrochemical Society, **159** (9) H735-H739 (2012)
0013-4651/2012/159(9)/H735/5/$28.00 © The Electrochemical Society

Zn-Doped SnO_2 Nanocrystals as Efficient DSSC Photoanode Material and Remarkable Photocurrent Enhancement by Interface Modification

Xincun Dou,[z] Rajiv Ramanujam Prabhakar, Nripan Mathews, Yeng Ming Lam,[z] and Subodh Mhaisalkar

Energy Research Institute @ NTU, School of Materials Science and Engineering, Nanyang Technological University, Singapore 639798

Zn-doped SnO_2 nanocrystals with different doping concentrations were synthesized and the nanocrystal photoanode based DSSC achieved a PCE of 2.07% with a high V_{oc} (0.67 V). $TiCl_4$ modification of the photoanode greatly improves the charge injection efficiency and charge collection efficiency and the resulting PCE increased to 4.32% despite a decreased dye adsorption. The Zn-doped SnO_2 nanocrystals will be of particular interest as photoanode material in DSSCs.
 [DOI: 10.1149/2.032209jes]

Manuscript submitted April 25, 2012; revised manuscript received June 7, 2012. Published August 14, 2012.

Nanocrystalline TiO_2, ZnO and SnO_2 have been studied extensively for use as photoanode materials in high performance dye sensitized solar cells (DSSCs).[1–10] Various morphologies of these photoanode materials have been synthesized with the aim of improving the dye adsorption and the light harvesting properties.[11,12] To date, the most efficient DSSCs are based on TiO_2 nanoparticle photoanodes (power conversion efficiency, PCE∼11%).[13,14] SnO_2 (E_g = 3.6 eV) is ideally suited for DSSCs due to its chemical stability and high electron mobility (∼100–200 $cm^2V^{-1}s^{-1}$) in comparison to nanocrystalline TiO_2 (∼10^{-2} $cm^2V^{-1}s^{-1}$).[15] However, when combined with the iodide/triiodide redox couple (I^-/I_3^-), the open circuit voltage (V_{oc}) is fairly low in a SnO_2-based DSSC (0.45 V).[16] A coral-like porous SnO_2 hollow architecture based DSSC obtained a V_{oc} of 0.52 V and PCE of 1.04%.[17] To the best of our knowledge, the latest reported efficiency for a N719 dye-sensitized SnO_2 DSSC was 3.16% with a V_{oc} of 0.503 V.[18]

As a result, the most immediate need for SnO_2 based DSSC is to improve the V_{oc} and the PCE. It was well known that PCE is not only affected by the light harvesting efficiency (η_{LH}), but also by the charge injection efficiency (η_{INJ}) and charge collection efficiency (η_{COL}).[19] The enhancement of electron injection from the dye excited state into the metal oxide electrode is especially important.[20] Previous results showed that using $TiCl_4$ treatment of the photoanode, a thin layer of TiO_2 nanoparticles were coated on the photoanode, enhancing the dye adsorption and thus enhance the light harvesting efficiency.[4] It was also shown that the metal oxide (Al_2O_3,Cr_2O_3,TiO_2,NiO, CuO, ZnO, MgO) passivation layer helps to increase the current density by the suppression of electron back transfer from SnO_2 to the redox electrolyte (I_3^-).[21–25] Hence, surface modification of the photoanodes would be an ideal strategy to improve the η_{LH} and η_{INJ}.[26]

In this work, we aim to improve the V_{oc} and short circuit current density (j_{sc}) of the SnO_2 nanocrystal photoanode based DSSC through Zn doping. As far as we know, the doping method (by adding urea or Hexamethylenetetramine (HMT) in the precursor) has never been reported previously and the doping concentration controlling is really novel. The obtained Zn-doped SnO_2 nanocrystals have high surface area (∼ 100 m^2/g), and the resulting DSSCs achieved a power conversion efficiency of 2.07% with a very high V_{oc} of 0.67 V. Further improvement of the PCE can be achieved by post surface modification of the photoanodes. However, it is found that this surface modification reduced the surface area of the photoanode (dye adsorption) but increased the PCE. The surface area decreased with $TiCl_4$ modification and PCE increased upon decreased adsorbed dye are completely new compared to all the previous results. It is found that the $TiCl_4$ modification of the Zn-doped SnO_2 nanocrystal photoanode greatly improves the charge injection from dye to photoanode due to increase of electron lifetime. Also it is found that the charge collection efficiency is enhanced due to the reduced contact resistance between the nanocrystals and FTO substrate.

Experimental

Synthesis of Zn-doped SnO_2 nanocrystals.— The SnO_2 nanocrystals was prepared by a hydrothermal method. Typically, a 30 mL mixture of equal amount of ethanol and DI water containing 1.0 mmol $Zn(CH_3COO)_2 \cdot 2H_2O$ and 1.0 mmol $SnCl_4$ is used for the synthesis of pure SnO_2 nanocrystals. Urea (1.0 g) or HMT (Hexamethylenetetramine, 1.0 g) was added to the above solution to achieve the 20% and 30% Zn-doped SnO_2 nanocrystals (determined by EDS). The solution was then transferred into a 50 mL Teflon-lined autoclave and was kept at 180°C for 24 hrs. The precipitate was collected after centrifugation and washed with distilled water and ethanol for several times. Finally, the product was dried completely at 70°C.

Electrode preparation and DSSC fabrication.— Paste making and DSSC fabrication were done according to the standard DSSC fabrication procedure.[14] The $TiCl_4$ modification of the Zn-doped SnO_2 nanocrystal film was performed by immersing the film into a 40 mM $TiCl_4$ aqueous solution for 30 min at 70°C. Then the electrodes were washed with ethanol and sintered at 500°C in air for 30 min. 0.5 mM of N719 dye was added to a solution with equal amount of tert-butanol and acetonitrile for the dye adsorption (20∼24 hrs, room temperature). For counter electrode preparation, Pt catalyst was deposited on cleaned FTO glass by coating with a drop of $H_2PtCl_6 \cdot 6H_2O$ solution (8 mM in ethanol) and then heated at 400°C for 15 min. Iodide based low viscosity electrolyte with 50 mM of tri-iodide in acetonitrile (AN-50, Solaronix) was used as the electrolyte.

Characterization.— Powder X-ray diffraction (Bruker D8 Advance), field emission scanning electron microscopy (FESEM; JEOL JSM-7600F), EDS, Nitrogen adsorption–desorption (Nova 3200e; quantachrome instruments), UV-Vis (Shimadzu 3600 Uv-Vis Spectrophotometers), Micro-photoluminescence (PL) system (Renishaw Raman Scope 2000) with a He-Cd laser (λ = 325 nm) as excitation source were used to characterize the nanocrystals. Dye desorption was conducted using a 20 mM NaOH solution (equal amount of DI water and ethanol) and by the absorption peak of N719 dye at 511 nm. The current density–voltage (J-V) characterization of DSSCs was performed under 1 sun condition using a solar light simulator (Oriel, 91160, AM 1.5 globe, 100 mW/cm^2). EIS spectrum[27] were collected using an Autolab potentiostat/galvanostat and the Nova 1.5 software package under illumination provided by a red LED (λ) 627 nm, 19.2 nm FWHM) while the cell was biased at the V_{OC} induced by the illumination.

[z]E-mail: xcdou@ms.xjb.ac.cn; YMLam@ntu.edu.sg

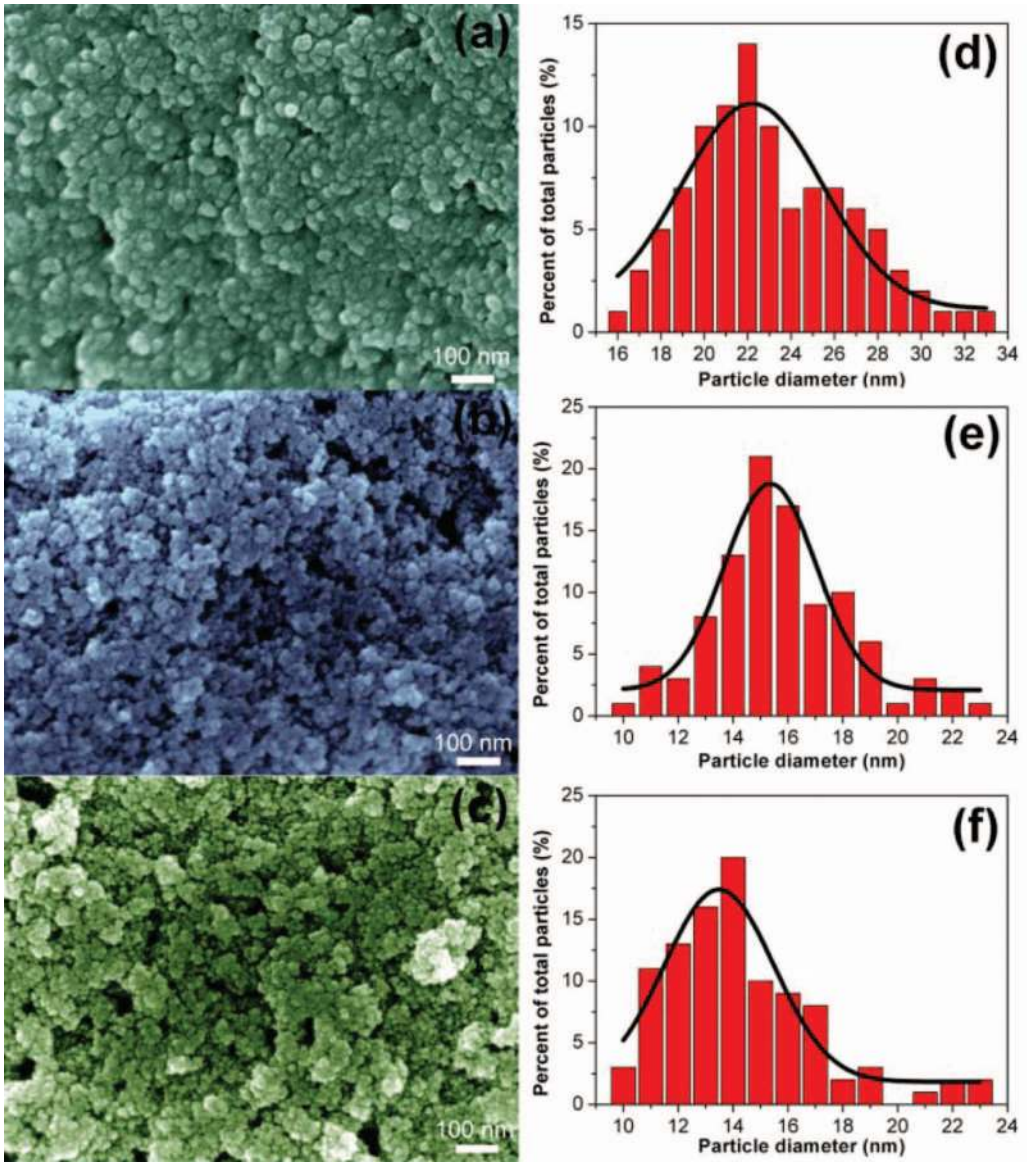

Figure 1. SEM images of (a) pure SnO_2 nanocrystals, (b) 20% Zn-doped SnO_2 nanocrystals, (c) 30% Zn-doped SnO_2 nanocrystals, and the respective particle size distributuion (d-f).

Results and Discussion

To characterize the morphology of the obtained nanocrystals, FE-SEM images of the different nanocrystals were taken (Fig. 1a-1c). The average sizes of the nanocrystals were obtained by counting the size of 100 nanocrystals and by Gauss fitting (Fig. 1d-1f). The average size of the pure SnO_2 nanocrystals was around 22 nm (Fig. 1d). The average sizes of the 20% and 30% Zn-doped SnO_2 nanocrystals were smaller and showed a fairly uniform size distribution of about 15 nm (Fig. 1e) and 14 nm (Fig. 1f). The surface area of the pure SnO_2, 20% and 30% Zn-doped SnO_2 nanocrystals were 91.4, 100.5 and 106.2 m^2/g respectively.

XRD patterns of the three kinds of SnO_2 nanocrystals (Fig. 2a) can be indexed to tetragonal phase of SnO_2 (JCPDS, 41-1445). The peaks of Zn-doped SnO_2 nanocrystals showed a slight shift to smaller angles, which was a result of Zn doping. The peaks of the Zn-doped SnO_2 nanocrystals broadened in comparison to that of the pure SnO_2 nanocrystals. This can be attributed to the decrease in crystal size of the Zn doped SnO_2 nanocrystals. The defects induced by Zn doping was evident from the photoluminescence spectrum of the Zn doped SnO_2 (Fig. 2b). The photoluminescence intensity of the defect emission increased with increasing Zn doping concentration. The UV-Vis absorption spectrum (Fig. 2c) and the bandgap calculation (Fig. 2d) showed that the pure SnO_2 nanocrystals had a bandgap of 4.07 eV, while the 20% and 30% Zn-doped SnO_2 nanocrystals showed a much smaller bandgap of 3.24 and 3.42 eV respectively. The reduced bandgap is considered to be caused by the doping effect. The increase of the bandgap with the increase of the doping concentration was reported previously in Zn-doped SnO_2 thin films.[28]

The doping mechanism can be considered as a slow hydrolysis of NH_3 given by the additives. When urea or HMT was introduced into the solution, they dissolved and formed ammonium hydroxide. The hydroxide anions in the solution reacted with tin and zinc ions and a white precipitate of $ZnSn(OH)_6$ was formed. Under high temperature and high pressure, further reaction occurred and Zn-doped SnO_2 was formed.[29]

To demonstrate the effect of Zn doping on DSSC performance, the 20% Zn-doped SnO_2 nanocrystals was made into paste and used as the photoanode of DSSC (with thickness of 8 and 10 μm). For both thicknesses, the effect of $TiCl_4$ modification was also studied. The J-V characteristics of the Zn-doped SnO_2 nanocrystal DSSCs were

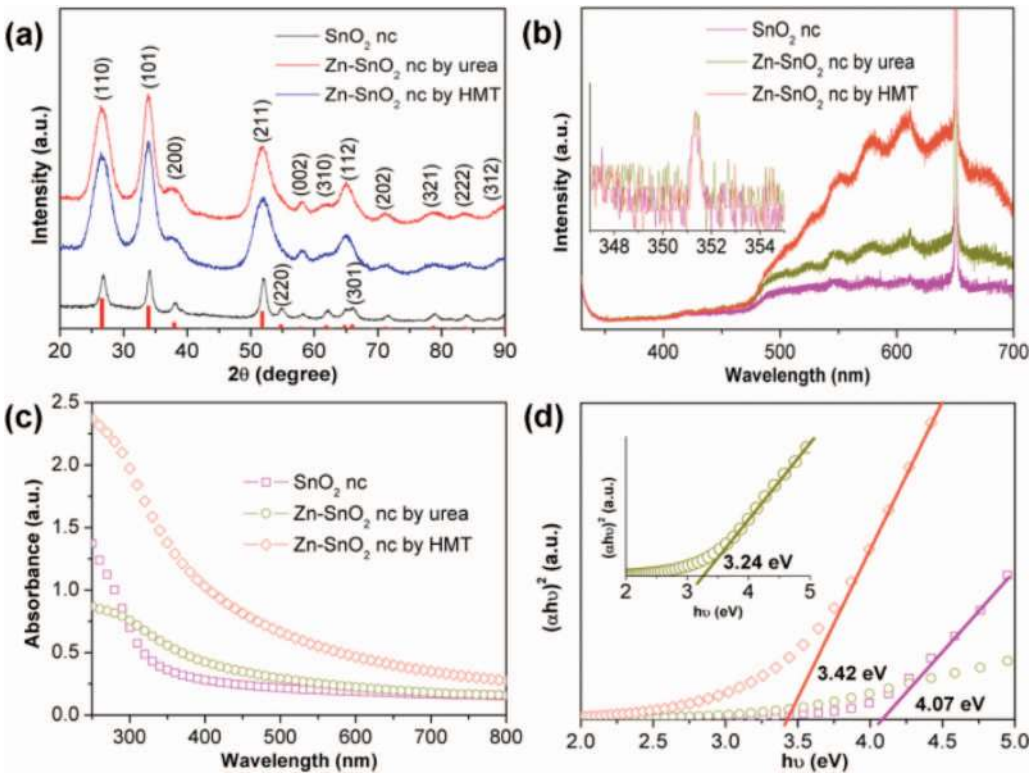

Figure 2. (a) XRD patterns and tetragonal SnO_2 (JCPDS, 41-1445) as a reference, (b) photoluminescence spectrum, (c) UV-Vis absorption spectrum, and (d) bandgap calculation of the three kinds of nanocrystals.

shown in Fig. 3. The V_{oc} of the 20% Zn-doped SnO_2 nanocrystals based DSSC (0.68 V) was much higher than the previously reported V_{oc} based on SnO_2 (0.52 V; with N719 dye).[17] Since n-type doping causes the Fermi level of SnO_2 to shift toward the conduction band, the high V_{oc} obtained here is due to the larger energy level offset between the Fermi level in Zn-doped SnO_2 with the reduction potential of I^-/I_3^- compared with pure SnO_2. The Zn-doped SnO_2 nanocrystal film with a 10 μm thickness showed a better dye adsorption than the P25 film with the same thickness (1.154×10^{-7} mol/cm^2).[4] The obtained PCE prior to $TiCl_4$ modification reaches 2.07% for the 10 μm thick photoanode, which was much higher than the other SnO_2 based systems.[17] After $TiCl_4$ modification of the photoanode, the V_{oc} increases 0.02 V and the current density doubled (from 4.85 to 10.33 mA/cm^2) and the highest efficiency reached 4.32%.

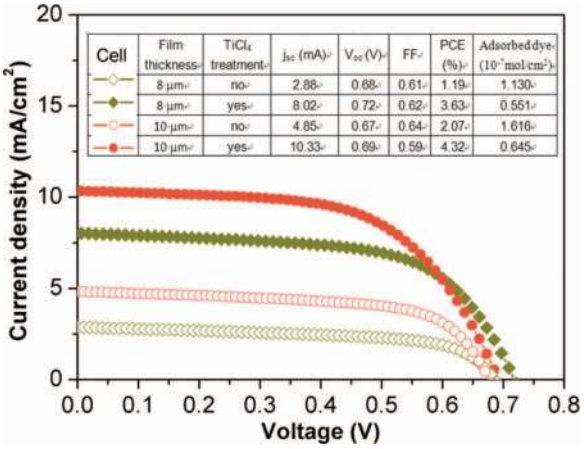

Cell	Film thickness	$TiCl_4$ treatment	j_{sc} (mA)	V_{oc} (V)	FF	PCE (%)	Adsorbed dye (10^{-7} mol/cm^2)
	8 μm	no	2.88	0.68	0.61	1.19	1.130
	8 μm	yes	8.02	0.72	0.62	3.63	0.551
	10 μm	no	4.85	0.67	0.64	2.07	1.616
	10 μm	yes	10.33	0.69	0.59	4.32	0.645

Figure 3. J-V characteristics of the DSSCs using 20% Zn-doped SnO_2 nanocrystals photoanode (8 μm or 10 μm) with/without $TiCl_4$ modification under AM 1.5G simulated sunlight with a power density of 100 mWcm^{-2}. (The active areas of the photoanodes are 0.2826 cm^2.)

Usually, the $TiCl_4$ modification helps to increase the dye loading, and thus helps to improve the light harvesting efficiency.[23] However, the dye adsorbed was found decreased by more than 50% with the $TiCl_4$ modification in the present study (Table in Fig. 3), which is different from most of other studies. Fig. 4a shows the linear relation between the dye concentration and the intensity of the absorption peak of N719 dye at 511 nm. Fig. 4b shows the UV-Vis absorption spectrum of the photoanodes with or without $TiCl_4$ modification. It is clearly shown that the absorption intensity decreased upon $TiCl_4$ modification. Since a thin TiO_2 layer formed on the surface of the nanocrystals after $TiCl_4$ modification,[23] the decrease of the dye adsorption is likely due to the drastic reduction in the spacing between the nanocrystals and thus the dye molecules could not penetrate deeper into the photoanode layer. As a result, the light harvesting efficiency decreased.

To study the effect of $TiCl_4$ modification on the kinetics of the charge transport and transfer in the 20% Zn-doped SnO_2 nanocrystal photoanode, EIS spectrum were obtained and fitted by using ZView software with an equivalent circuit (inset in Fig. 5a) which is based on the general transmission line model of DSSC.[30] Fig. 5a and 5b show the typical Nyquist plots of the Zn-doped SnO_2 nanocrystal photoanode (10 μm in thickness; without or with $TiCl_4$ modification) based DSSCs at two open circuit voltages. In all the EIS spectra, two well-defined semicircles were observed in the high frequency region (>1 kHz) and in the frequency region of 0.1∼100 Hz, respectively. Based on the general transmission line model of DSSC and the equivalent fitting circuit (inset in Fig. 5a),[30] the diameter of the first semicircle in the Nyquist plot is related to R_{Pt}, R_{FTO} and $R_{contact}$, which represents the charge-transfer resistance at the counter electrode, the exposed FTO-electrolyte interface and the FTO-SnO_2 nanocrystal contact respectively. It is obvious that the diameter of the first semicircle increases greatly with the decrease of the applied voltage from 0.67 V to 0.64 V (Fig. 5a, without $TiCl_4$ modification). While the diameter of

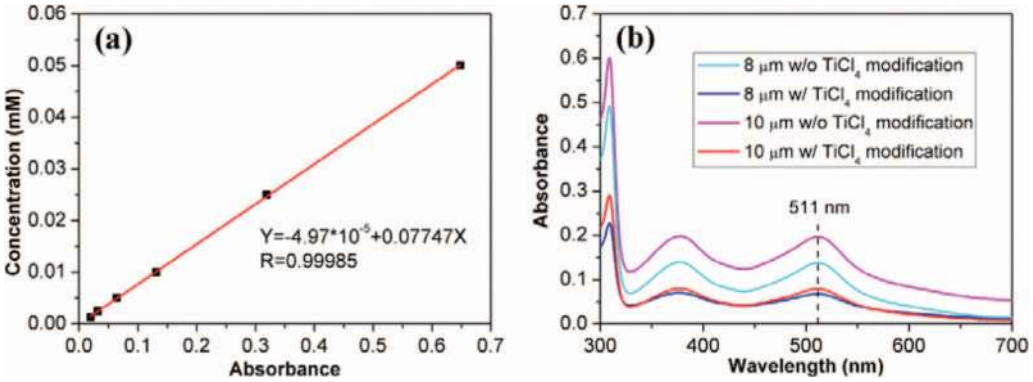

Figure 4. (a) Linear relation between the N719 dye concentration and the intensity of the absorption peak at 511 nm. (b) UV-Vis absorption spectrum of the 8 μm and 10 μm thick photoanodes with or without $TiCl_4$ modification.

the first semicircle increases very slowly with the decrease of the applied voltage from 0.67 V to 0.63 V (Fig. 5b, with $TiCl_4$ modification). Compare the cell configurations and the EIS spectrum of the Zn-doped SnO_2 nanocrystal photoanode (without or with $TiCl_4$ modification) based DSSCs, the following characteristics can be found. The charge-transfer resistance at the counter electrode (R_{Pt}) is the same for both of the DSSCs with or without $TiCl_4$ modification of the photoanode. Since the electrolyte and the FTO keep unchanged, the charge-transfer resistance at the exposed FTO-electrolyte interface (R_{FTO}) also remians not changed. The only change induced by $TiCl_4$ modification is the charge-transfer resistance at the FTO-SnO_2 nanocrystal contact, which is denoted as the contact resistance ($R_{contact}$). As a result, the change of the diameter of the first semicircle in the Nyquist plot is induced largely by the change of $R_{contact}$. The contact resistance of the 20% Zn-doped SnO_2 nanocrystal films increased largely with the decrease of V_{oc} (Fig. 5c). It is obvious that $TiCl_4$ modification greatly helps to decrease the contact resistance (Fig. 5c). The decrease of the contact resistance will improve the charge collection efficiency. The $TiCl_4$ modification will help to form a very thin layer of TiO_2 film on the entire surface of the photoanode.[23] In addition, the $TiCl_4$ modification will definitely help to increase the contact area between Zn-doped SnO_2 nanocrystals and FTO substrate, as illustrated in Fig. 5d. As a result, the charge-transfer resistance at the FTO-SnO_2 nanocrystal contact ($R_{contact}$) decreased greatly upon $TiCl_4$ modification.

The second semicircle denotes the electron transfer at the oxide/dye/electrolyte interface. By fitting the Nyquist plot, the electron transfer information can be interpreted. The chemical capacitance (C_μ) increased at least 10 times after $TiCl_4$ modification (Fig. 6a). It is considered that the surface states greatly increased due to the $TiCl_4$ modification and these surface states helped to capture the electrons injected by the excited dye molecules rather than facilitate the recombination of injected electrons back to the redox electrolyte.[30–32]

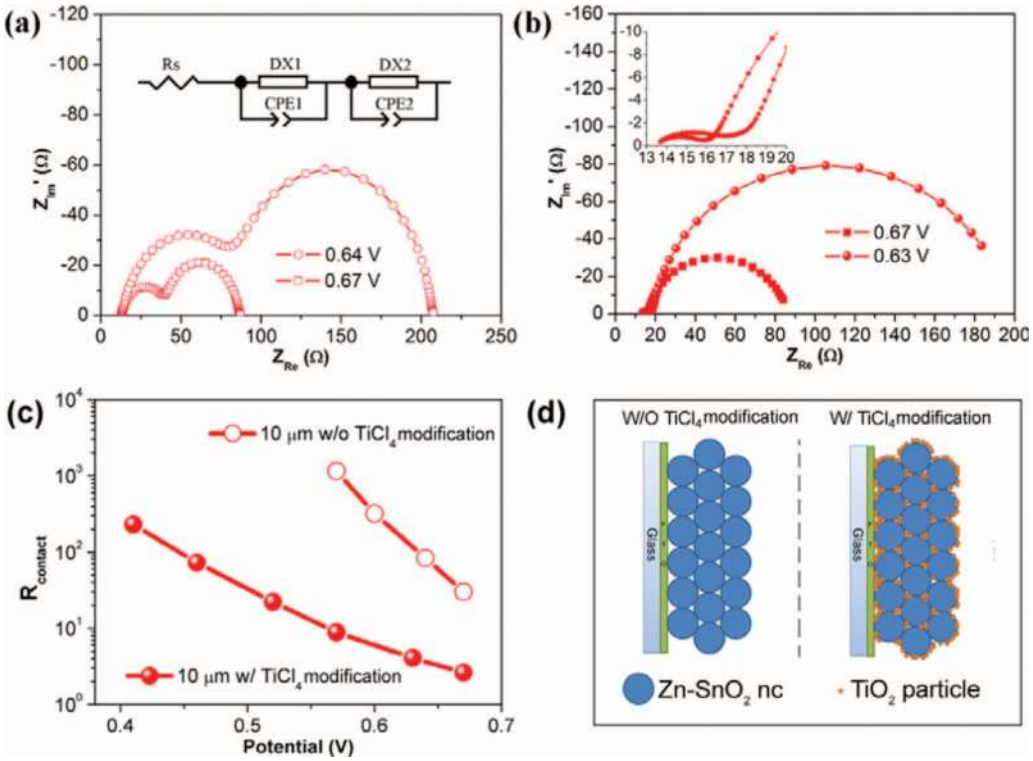

Figure 5. Nyquist plots of the 20% Zn-doped SnO_2 nanocrystal photoanode (10 μm in thickness) based DSSCs without (a) or with (b) $TiCl_4$ modification at different V_{oc}. The inset in (a) is the equivalent circuit used to fit the EIS spectra. The inset in (b) is the enlarged Nyquist plots. (c) The charge-transfer resistance at the FTO-SnO_2 nanocrystal contact ($R_{contact}$) with a function of applied potential. (d) The schematic graphs of the photoanode with/without $TiCl_4$ modification.

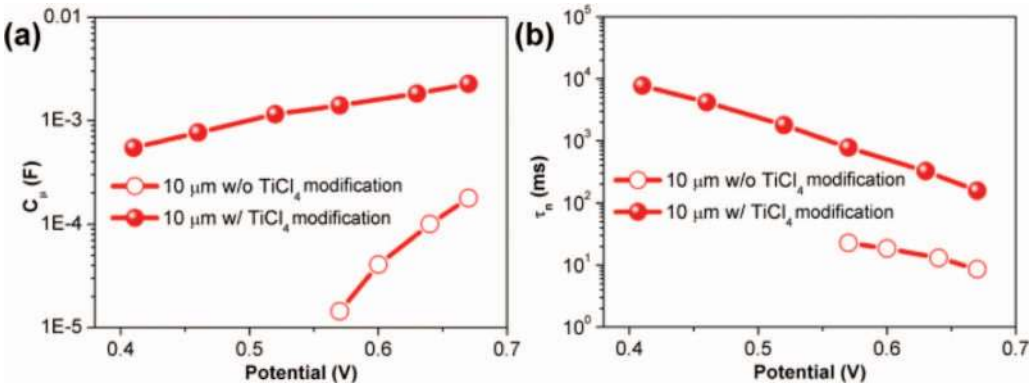

Figure 6. (a) The chemical capacitance C_μ, (b) the electron lifetime τ_n of the DSSCs using 20% Zn-doped SnO_2 nanocrystals photoanode (10 μm in thickness) with/without $TiCl_4$ modification.

The electron lifetime (τ_n) of the Zn-doped SnO_2 nanocrystal photoanode DSSC also increased at least 10 times after $TiCl_4$ modification (Fig. 6b). The larger the electron lifetime, the slower the recombination rate.[4] As a result, $TiCl_4$ modification which increased the electron lifetime will make the recombination rate slower. The charge injection efficiency after $TiCl_4$ modification was greatly improved.[31]

Conclusions

In conclusion, for the first time Zn-doped SnO_2 nanocrystals with different doping concentrations were successfully synthesized and were used as a photoanode in DSSCs. Compared to the previous pure SnO_2 nanostructures based DSSCs with N719 dye as the sensitizer, the present Zn-doped SnO_2 nanocrystals based DSSC achieved an efficiency of 2.07% and a high V_{oc} of 0.67 V. $TiCl_4$ modification of the Zn-doped SnO_2 nanocrystal photoanode greatly improves the charge injection efficiency (due to increase of electron lifetime) and the charge collection efficiency (due to the reduced contact resistance between the nanocrystals and FTO substrate). As a result, the photocurrent doubled and PCE reaches 4.32% despite a decreased dye adsorption. The Zn-doped SnO_2 nanocrystals will be of particular interest as photoanode material in DSSCs.

Acknowledgments

This work is supported by the National Research Foundation, Singapore (CRP).

References

1. B. O'Regan and M. Grätzel, *Nature*, **353**, 737 (1991).
2. P. Wang, S. M. Zakeeruddin, J. E. Moser, M. K. Nazeeruddin, T. Sekiguchi, and M. Grätzel, *Nat. Mater.*, **2**, 402 (2003).
3. F. Sauvage, F. Di Fonzo, A. L. Bassi, C. S. Casari, V. Russo, G. Divitini, C. Ducati, C. E. Bottani, P. Comte, and M. Grätzel, *Nano Lett.*, **10**, 2562 (2010).
4. J. F. Qian, P. Liu, Y. Xiao, Y. Jiang, Y. L. Cao, X. P. Ai, and H. X. Yang, *Adv. Mater.*, **21**, 3663 (2009).
5. J. C. Chou, Y. Y. Chiu, Y. M. Yu, S. Y. Yang, P. H. Shih, and C. C. Chen, *J. Electrochem. Soc.*, **159**, A145 (2012).
6. C. Lee, G. Lee, W. Kang, D. Lee, M. Ko, K. Kim, and N. Park, *Bull. Korean Chem. Soc.*, **31**, 3093 (2010).
7. W. H. Chen, A. G. Miranda, and C. W. Hong, *J. Electrochem. Soc.*, **158**, P57 (2011).
8. M. Wu, Y. Wang, X. Lin, N. Yu, L. Wang, L. Wang, A. Hagfeldt, and T. Ma, *Phys. Chem. Chem. Phys.*, **13**, 19298 (2011).
9. X. Chen and S. S. Mao, *Chem. Rev.*, **107**, 2891 (2007).
10. L. Li, T. Zhai, Y. Bando, and D. Golberg, *Nano Energy*, **1**, 91 (2012).
11. S. Chappel and A. Zaban, *Sol. Energy Mater. Sol. Cells*, **71**, 141 (2002).
12. R. Jose, V. Thavasi, and S. Ramakrishna, *J. Am. Ceram. Soc.*, **92**, 289 (2009).
13. Y. Chiba, A. Islam, R. Komiya, N. Koide, and L. Y. Han, *Appl. Phys. Lett.*, **88**, 223505 (2006).
14. S. Ito, T. N. Murakami, P. Comte, P. Liska, C. Gratzel, M. K. Nazeeruddin, and M. Grätzel, *Thin Solid Films*, **516**, 4613 (2008).
15. M. S. Arnold, P. Avouris, Z. W. Pan, and Z. L. Wang, *J. Phys. Chem. B*, **107**, 659 (2002).
16. S. Ferrere, A. Zaban, and B. A. Gregg, *J. Phys. Chem. B*, **101**, 4490 (1997).
17. J. Liu, T. Luo, S. M. T, F. Meng, B. Sun, M. Li, and J. Liu, *Chem. Commun.*, **46**, 472 (2010).
18. A. Birkel, Y.-G. Lee, D. Koll, X. V. Meerbeek, S. Frank, M. J. Choi, Y. S. Kang, K. Char, and W. Tremel, *Energ Environ Sci*, **5**, 5392 (2012).
19. J. Halme, P. Vahermaa, K. Miettunen, and P. Lund, *Adv. Mater.*, **22**, E210 (2010).
20. A. Listorti, B. O'Regan, and J. R. Durrant, *Chem. Mater.*, **23**, 3381 (2011).
21. A. Kay and M. Grätzel, *Chem. Mater.*, **14**, 2930 (2002).
22. C. Prasittichai and J. T. Hupp, *J. Phys. Chem. Lett.*, **1**, 1611 (2010).
23. E. Ramasamy and J. Lee, *J. Phys. Chem. C*, **114**, 22032 (2010).
24. S. Y. Choi, M. H. Kim, and Y. U. Kwon, *Phys. Chem. Chem. Phys.*, **14**, 3576 (2012).
25. C.-H. Lee, G.-W. Lee, W.-K. Kang, D.-K. Lee, M.-J. Ko, K.-K. Kim, and N.-G. Park, *Bull. Korean Chem. Soc.*, **31**, 3093 (2010).
26. H. J. Snaith and C. Ducati, *Nano Lett.*, **10**, 1259 (2010).
27. J. Bisquert, *J. Phys. Chem. B*, **106**, 325 (2001).
28. J. S. Bhat, K. I. Maddani, and A. M. Karguppikar, *Bull. Mater. Sci.*, **29**, 331 (2006).
29. Z. Li, X. Li, X. Zhang, and Y. Qian, *J. Cryst. Growth*, **291**, 258 (2006).
30. Q. Wang, S. Ito, M. Grätzel, F. Fabregat-Santiago, I. Mora-Seró, J. Bisquert, T. Bessho, and H. Imai, *J. Phys. Chem. B*, **110**, 25210 (2006).
31. X. C. Dou, D. Sabba, N. Mathews, L. H. Wong, Y. M. Lam, and S. Mhaisalkar, *Chem. Mater.*, **23**, 3938 (2011).
32. L. L. Lu, R. J. Li, T. Y. Peng, K. Fan, and K. Dai, *Renew. Energ.*, **36**, 3386 (2011).